CRYSTAL GROWTH & DESIGN

Article

Cite This: Cryst. Growth Des. 2017, 17, 6801−6808

pubs.acs.org/crystal

Fast Synthesis of Gibbsite Nanoplates and Process Optimization using Box-Behnken Experimental Design

Xin Zhang,*[,†] Xianwen Zhang,[‡] Trent R. Graham,[§] Carolyn I. Pearce,[†] B. Layla Mehdi,[†] Alpha T. N'Diaye,[∥] Sebastien Kerisit,[†] Nigel D. Browning,[†] Sue B. Clark,[†,⊥] and Kevin M. Rosso*[,†]

[†]Pacific Northwest National Laboratory, Richland, Washington 99352, United States

[‡]School of Automobile and Transportation Engineering, Hefei University of Technology, Hefei, Anhui 230009, China

[§]The Voiland School of Chemical and Biological Engineering and [⊥]Department of Chemistry, Washington State University, Pullman, Washington 99164, United States

[∥]Advanced Light Source, Lawrence Berkeley National Laboratory, Berkeley, California 94720, United States

Supporting Information

ABSTRACT: Developing the ability to synthesize compositionally and morphologically well-defined gibbsite particles with high yield is an ongoing need that has not yet achieved the required level of rational design. Here we report optimization of a clean inorganic synthesis route based on statistical experimental design examining the influence of $Al(OH)_3$ gel precursor concentration, pH, and aging time at temperature. At 80 °C, the optimum synthesis conditions of gel concentration at 0.5 M, pH at 9.2, and time at 72 h maximized the reaction yield up to ∼88%. The resulting gibbsite product is composed of highly uniform euhedral hexagonal nanoplates within a basal plane diameter range of 200−400 nm. The independent roles of key system variables in the growth mechanism are considered. On the basis of these optimized experimental conditions, the synthesis procedure, which is both cost-effective and environmentally friendly, has the potential for mass production scale-up of high quality gibbsite material for various fundamental research and industrial applications.

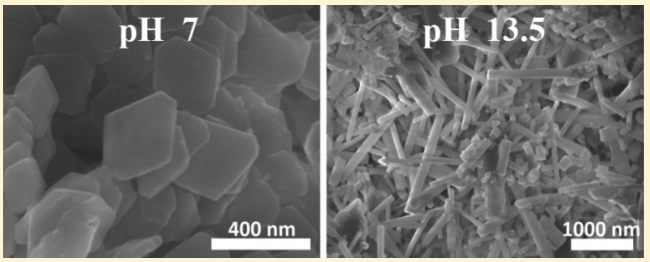

INTRODUCTION

Gibbsite, α-$Al(OH)_3$, is an important natural and industrial material that is used in a wide variety of applications including flame retardants, adsorbents, polishing agents, fillers, coating materials, and as a rheology enhancer.[1−5] Gibbsite has also been used in the biomedical industry, for instance, as a vaccine adjuvant and a substrate for direct treatment of stomach diseases.[6,7] Furthermore, gibbsite is one of the most important precursors for the preparation of various alumina products, such as high surface area α-Al_2O_3, which have a broad range of applications in the ceramics and metallurgical industries and as adsorbents or supports for catalysts.[3,8] Finally, gibbsite is a major constituent in high-level nuclear waste stored in large quantities at the Hanford Site, Washington, USA, and at the Savannah River Site, South Carolina, USA, with future processing plans dependent on developing a predictive understanding of the growth and dissolution behavior of this material in particular.[9]

In most cases, the chemical behavior of gibbsite in these systems depends strongly on its physical properties, such as particle size and shape. For example, in applications as an adsorbent, rheology enhancer, vaccine adjuvant, or as a precursor for the preparation of high surface area α-Al_2O_3, it is desirable for the gibbsite to be nanoscale.[3,8,10,11] Developing a fundamental understanding of gibbsite reactivity in complex systems such as nuclear waste, gaining precise control of particle crystallinity, size, morphology, and structural perfection of crystallite facets is critical.[3,11−21] Thus, there is an ongoing need for developing the ability to synthesize gibbsite materials that are nanoscale with uniform physical properties.

Gibbsite particles tend to adopt a platelet morphology. Gibbsite has a hexagonal crystal structure, comprised of quasi-two-dimensional layers of edge-sharing octahedral $Al^{3+}(OH)_6$ sheets each having two-thirds of the octahedral cavities occupied, and sheets are weakly bound together along the c-axis by hydrogen bonding (Figure S1). This structure thus tends to feature a dominant (001) basal surface bound by relatively stable (110) and (010) edge facets and less stable (100) facets.[22]

Synthesis is achievable through various routes. Typically it is prepared based on the industrial process of manipulating Bayer liquors.[14,16,19] Such gibbsite, usually several to hundreds of micrometers in size, shows very rough surfaces at the microscale.[14,16] Because Bayer liquors entail very high concentrations of sodium aluminate and typically contain impurities, these undesirable components comprise a large

Received: October 2, 2017
Revised: November 3, 2017
Published: November 13, 2017

DOI: 10.1021/acs.cgd.7b01400
Cryst. Growth Des. 2017, 17, 6801−6808

fraction of the adsorbed residual.[14,19] Recently, alternative synthesis protocols that more specifically emphasize size and shape control have been developed. For example, using more dilute sodium aluminate solution as the aluminum precursor, and adding a surfactant such as cetyltrimethylammonium bromide (CTAB) as a particle capping agent, prismatic "bar-shaped" gibbsite that is disproportionately extended along the *c*-axis and features prominent edge facets can be prepared hydrothermally.[23] However, the size of these bar-shaped particles (longest dimension along *c*-axis) was up to several micrometers, with a specific surface area too low for most applications.

The sensitive control of gibbsite physical properties available via synthesis with organic additives has led to exploration of these effects with promising albeit empirical results with unpredictable yields. For example, particles approaching the nanoscale can be prepared by a simple thermal treatment of aluminum alkoxides mixed with hydrochloric acid (HCl).[11,20,21,24] Generally, the procedure entails two steps: (1) obtain a clear sol via mixing an aqueous solution of aluminum alkoxides with HCl followed by stirring for 7−10 days at room temperature; (2) heat the sol solution to 100 °C for around 3 days to precipitate gibbsite with a yield of 41−66%. Typical products are nanoplates approximately 200 nm in diameter. However, this procedure is slow, consuming more than 10 days. A modified method shortens the synthesis period to 4 days by using a single aluminum alkoxide as the precursor and introducing an intermediate preheating step to accelerate the precursor's hydrolysis/peptization.[3] But, unfortunately, although again nanoplates approximately 200 nm in size result, the yield decreases to less than 30%. Incidentally, platelets of larger size (up to 1 μm) could be prepared by repeating the seed growth procedure (step two above). However, in all these cases with organic additives, similar to the case for CTAB, there is a purity concern for the platelet surfaces due to organic precursor residue.

For clean inorganic routes, the most flexible approach entails use of amorphous aluminum hydroxide [$Al(OH)_3$] gel as the precursor and control of the properties of the gibbsite product through aging time, temperature, and solution pH. Care must be taken in the gel preparation method, which can also influence the quality of the product. A gel, precipitated at 75 °C by adding ammonia aqueous to an aluminum nitrate hexahydrate [$Al(NO_3)_3{\cdot}6H_2O$] aqueous solution to adjust the pH up to 8, was aged at that temperature for more than 2 days and yielded irregular gibbsite particles 10−20 μm in diameter.[13] A similar gel, prepared by adding ammonia to an aluminum nitrate nonahydrate [$Al(NO_3)_3{\cdot}9H_2O$] aqueous solution, was titrated to pH 5 and aged at 100 °C for 10 days to yield uniform hexagonal gibbsite platelets 600−800 nm in size.[25] This modified procedure offered better quality gibbsite, but the product size was too big and the synthesis time too long for most applications. When the pH of the gel precursor was 7 and 10, the products were instead amorphous aluminum hydroxide or boehmite (γ-AlOOH) with minor amounts of bayerite, respectively.[25]

Smaller gibbsite nanoplates could be obtained by aging at lower temperature, but the working time was much longer and the yield low. For example, preparing the gel by mixing aluminum chloride ($AlCl_3$) and sodium hydroxide (NaOH) aqueous solutions at pH around 4.6 followed by aging at 70 °C[2,26] for 1−4 months or at 50 °C for 1−2 months[10,27] yielded gibbsite nanoplates with diameters of approximately 200−300 nm and 100−200 nm, respectively. This short review of previous work highlights the sensitivity of the gel-based approach to aging time, temperature, and pH. It also exemplifies the present lack of systematic understanding of the relative importance of these three master variables. Finally, with respect to production scale-up of nanoparticles with precisely defined sizes and shapes, all the above-mentioned methods have drawbacks related to the apparent inverse correlation between synthesis time and particle size.

A systematic study of the effects of major synthesis variables is required to achieve high yields while retaining size and shape control. In this study, we take advantage of statistical experimental design via the Box-Behnken strategy[28,29] to gain insight into the most important synthesis variables with respect to size, shape, and yield. The result of this effort is a simple and optimized hydrothermal method to fast-synthesize euhedral hexagonal gibbsite nanoplates with diameters from 200 to 400 nm and thicknesses from 8 to 20 nm. The synthesis approach consists of reacting a $Al(OH)_3$ gel precursor, prepared by adding NaOH (aq.) to $Al(NO_3)_3{\cdot}9H_2O$ (aq.), at 80 °C for 72 h. The effect of aging temperature and time, pH and precursor concentration on the size and morphology of gibbsite and product yield was studied in detail. Furthermore, the product yield achievable via this synthesis route was maximized to 88% through statistical experimental design. Confirmatory evidence for the formation of high-quality gibbsite nanoplates was obtained using powder X-ray diffraction (XRD), scanning electron microscopy (SEM), scanning/transmission electron microscopy (S/TEM), synchrotron X-ray absorption spectroscopy (XAS), and atomic force microscopy (AFM).

EXPERIMENTAL METHODS

Synthesis of Gibbsite Nanoplates. Samples were grown using a hydrothermal method. $Al(NO_3)_3{\cdot}9H_2O$ (≥98%, Sigma-Aldrich) was dissolved into deionized water under stirring to form a homogeneous solution with a concentration of 0.25 M at room temperature, followed by addition of 1 M NaOH (≥98%, Sigma-Aldrich) aqueous solution to adjust the pH to around 5.0. After continuous stirring for 1 h, the solution was centrifuged to collect gel-like precipitates. The gel was washed with deionized water three times. Gels were dispersed into water solution with pH from 1−13.5 (HCl for acid and NaOH for base) and then the solution was transferred to a 20 mL Teflon vessel. The concentration of gels (defined as the concentration of Al^{3+}) ranged from 0.1 to 1 M, and the volume of the gel solution was 16 mL. The Teflon vessel was sealed within a Parr bomb and heated in an electric oven with rotator at 60−100 °C for 12−96 h. The rotation speed was around 10 rpm. The resulting white product was recovered by centrifuging and washing with deionized water three times. The solid sample obtained was dried at 80 °C overnight. Samples were characterized by various techniques including XRD, S/TEM, SEM, XAS and AFM.

X-ray Diffraction. XRD patterns of the samples were recorded on a Philips X'pert Multi-Purpose diffractometer (MPD) (PANAlytical, Almelo, The Netherlands) equipped with a fixed Cu anode operating at 50 kV and 40 mA. XRD 2θ values varied between 5−60°. Phase identification was performed using JADE 9.5.1 from Materials Data Inc., and the 2012 PDF4+ database from International Center for Diffraction Data (ICDD) database.

Scanning Electron Microscopy. The morphologies of as-prepared gibbsite samples were examined using a Helios NanoLab 600i SEM (FEI, Hillsboro, OR). All samples were sputter coated with a 5 nm layer of carbon to ensure good conductivity and imaging.

Scanning/Transmission Electron Microscopy. As-prepared gibbsite samples were dispersed in water using a sonicator for 5 min. Samples for TEM (FEI Titan TEM) examination were prepared by placing drops of aqueous gibbsite dispersions onto the copper grid

DOI: 10.1021/acs.cgd.7b01400
Cryst. Growth Des. 2017, 17, 6801−6808

Table 1. Overview of Gibbsite Synthesis Conditions and Resulting Products

entry	concentration (M)	pH	temp (°C)	time (h)	product	morphology	yield (%)
1	0.5	7	60	72	amorphous gel with minor gibbsite	nanoparticles with minor hexagonal nanoplates	25.2
2	0.5	7	70	72	amorphous gel with minor gibbsite	nanoparticles with minor hexagonal nanoplates	36.8
3	0.5	7	80	72	gibbsite	hexagonal nanoplates	82.6
4	0.5	7	90	72	gibbsite	hexagonal nanoplates	84.3
5	0.5	7	100	72	gibbsite	hexagonal nanoplates	83.6
6	0.5	7	80	12	trace solids		
7	0.5	7	80	24	trace solids		
8	0.5	7	80	48	gibbsite	hexagonal nanoplates	29.2
9	0.5	7	80	96	gibbsite	hexagonal nanoplates	83.2
10	0.5	1	80	72	gibbsite	hexagonal nanoplates	36.5
11	0.5	3	80	72	gibbsite	hexagonal nanoplates	68.2
12	0.5	5	80	72	gibbsite	hexagonal nanoplates	76.6
13	0.5	10	80	72	gibbsite	hexagonal nanoplates	83.9
14	0.5	12	80	72	gibbsite	hexagonal nanoplates	84.8
15	0.5	13.5	80	72	70% gibbsite, 30% bayerite	nanorods with irregular nanoparticles	88.5
16	0.1	7	80	72	gibbsite	hexagonal nanoplates	56.2
17	0.25	7	80	72	gibbsite	hexagonal nanoplates	80.6
18	0.75	7	80	72	gibbsite with trace amorphous gel	hexagonal nanoplates with nanoparticles	76.5
19	1	7	80	72	gibbsite with trace amorphous gel	hexagonal nanoplates with nanoparticles	50.2

(Lacey Carbon, 300 mesh, Copper, Ted Pella, Inc.), which was then dried under ambient conditions prior to being introduced into the TEM chamber. The samples were imaged using an acceleration voltage of 300 kV.

The S/TEM samples were prepared by drop-casting suspension of as-prepared gibbsite samples dispersed in ethanol onto the copper grid. The STEM images were taken with aberration-corrected FEI Titan 80−300 operating at 300 keV in STEM mode with high angle annular dark field (HAADF) detector. The inner collection angle was ∼75 mrad, and the nominal probe size was ∼0.1 nm. All images were taken under a low dose condition to avoid electron beam damage.

Synchrotron X-ray Absorption Spectroscopy (XAS). Al and O K-edge X-ray absorption spectroscopy (XAS) data for gibbsite were measured on Beamline 6.3.1.1 at the Advanced Light Source (Berkeley, CA). A powdered sample was pressed into indium foil and mounted onto a copper sample probe using silver paint. The XAS signal was monitored at room temperature using total-electron-yield (TEY) mode with an effective probing depth of ∼4.5 nm. A reference spectra of corundum (α-Al_2O_3) was used to calibrate the energy scale.[30] The photon energy resolution value for Al K-edge spectroscopy was 0.75 eV.

Atomic Force Microscope. The thickness of as-prepared gibbsite nanoplates was measured with a Dimension Icon AFM (Bruker, USA) operating in contact mode. All images were collected with standard silicon nitride tips with Au conductive coating (MLCT, Bruker, USA) at a scan rate of 1 Hz with 512 × 512 lines scan. All samples were made by placing drops of gibbsite/water suspensions onto silicon substrates and removing the solution after several minutes. The substrate was then washed several times using DI water and dried using high-purity nitrogen. Polished silicon wafers were purchased from Nova Electronic Materials Ltd. The diced silicon substrates were washed twice with DI water and then sonicated in ethanol for 5 min. Finally, the diced silicon substrates were treated using plasma cleaner for 30 min under Ar followed by ozone cleaner for 30 min before use.

Box-Behnken Design (BBD). The BBD of reaction yield optimization allows a prediction of the combined effects of three controlled factors of 15 runs, as shown in Table S1.[28,29] Three levels were attributed to each factor, coded as −1 (low), 0 (medium), and +1 (high). Runs 7, 8, and 11 were performed with the variable parameters at the middle level (center point runs). BBD is an independent quadratic design in that it does not contain an embedded factorial or fractional factorial design. In this design, the treatment combinations are at the midpoints of edges of the process space and at the center. These designs are rotatable and require three levels of each factor. The designs have limited capability for orthogonal blocking compared to the central composite designs.

The adequacy of the models and statistically significant terms were identified by the analysis of variance (ANOVA) of BBD. ANOVA was performed at an alpha level of 0.05 to evaluate the significance of second-order model. The F statistic and lack-of-fit test were obtained to determine if the regression models were adequate to fit the data.

RESULTS AND DISCUSSION

Effect of Temperature. We first examined the effect of temperature on the synthesis of gibbsite. Temperature modulates the extent of supersaturation and also affects crystal growth kinetics.[18,31] As shown in Table 1 (entries 1−5) five different temperatures of 60, 70, 80, 90, and 100 °C were investigated, using an initial reaction time of 72 h and an initial pH of 7.0. In each case, XRD was used to check phase purity and crystallinity of the samples, as shown in Figure 1. Products prepared at low temperature (60 and 70 °C) contained an amorphous phase, which not only appeared in the XRD patterns (Figure 1a,b) but was also identifiable in TEM selected area electron diffraction (SAED) analysis (Figure 2a−c for 60 °C and Figure 2d−e for 70 °C). Furthermore, the gibbsite yield

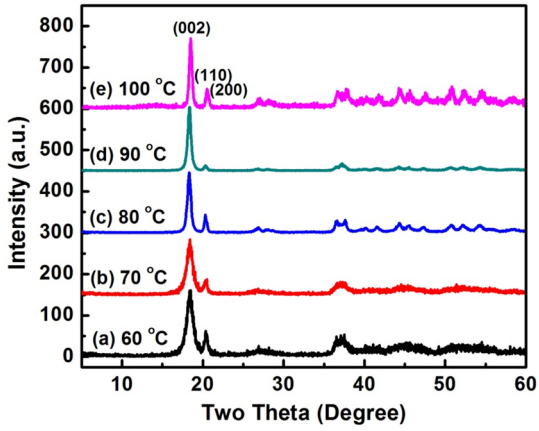

Figure 1. XRD patterns of gibbsite after 72 h synthesized at different temperatures: (a) 60; (b) 70; (c) 80; (d) 90; and (e) 100 °C.

DOI: 10.1021/acs.cgd.7b01400
Cryst. Growth Des. 2017, 17, 6801−6808

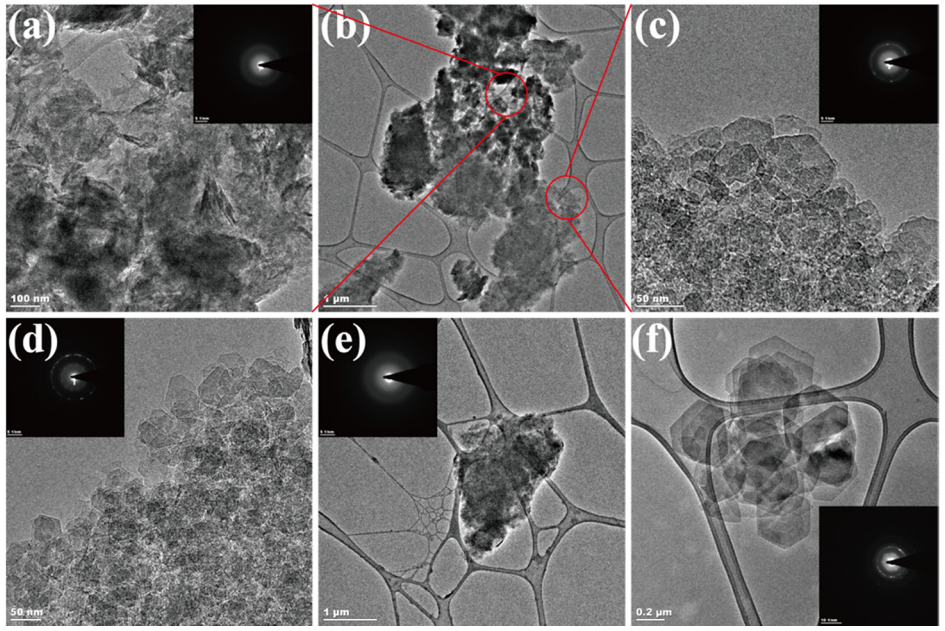

Figure 2. TEM and diffraction data of gibbsite after 72 h synthesized at different temperatures: (a–c) 60; (d) and (e) 70; and (f) 80 °C.

was less than 40% for these two lowest temperatures (Table 2, entries 1 and 2). However, products prepared at higher temperatures (80, 90, and 100 °C) were pure gibbsite, as determined based on both XRD (Figure 1c–e) and TEM SAED analysis (Figure 2f), and the yield was greater than 80% (Table 1, entries 3–5). The diffraction pattern is in good agreement with reference data for gibbsite (ICDD PDF # 00-33-0018).[23,25] The strong diffraction peak at the 2θ angle of 18.29 is assigned to (0 0 2) diffraction, based on the atomic structure along the plane normal (Figure S1). To quantify the degree of crystallization, peak fitting was carried out as a proxy for the measure of crystallinity through determination of full-width-at-half-maximum (fwhm). As shown in Figure S2, the phase composition of gibbsite is around 30% and 85% when the hydrothermal temperature is 60 and 70 °C, respectively; however, 100% gibbsite is obtained when the temperature is higher than 80 °C.

Table 2. Box-Behnken Design and Result

entry	concentration (M)	pH	reaction time (h)	reaction yield (%)
1	0.35	12	72	47.85
2	0.5	8.5	72	86.69
3	0.2	8.5	40	26.44
4	0.5	5	56	43.27
5	0.5	12	56	34.29
6	0.35	12	40	6.30
7	0.35	8.5	56	42.12
8	0.35	8.5	56	44.64
9	0.35	5	40	11.68
10	0.2	8.5	72	81.73
11	0.35	8.5	56	47.39
12	0.5	8.5	40	8.81
13	0.2	12	56	30.47
14	0.35	5	72	70.17
15	0.2	5	56	41.47

Surface sensitive Al K-edge XAS was used to probe the bonding and symmetry of the local environment around the Al atoms within ~4.5 nm of the gibbsite surface. The Al K-edge XAS spectrum of the synthetic gibbsite synthesized at 80 °C (Figure 3a) consists of a broad peak (~8 eV wide), with two distinguishable absorption features: one feature (I) is a shoulder at 1568 eV and the other (II) is a broad, intense feature at 1570 eV, in good agreement with previously reported gibbsite spectra.[30,32] These features arise from the gibbsite structure, which consists of octahedral layers with two Al sites located in distorted octahedra and Al–O distances from 1.832 to 1.947 Å.[33] The O K-edge XAS spectrum of gibbsite (Figure 3b) is sensitive to the O bonding environment at the surface and arises from O 1s transition to O 2p unoccupied states mixed with the ligand s, p, and sp orbitals.[34] There are two distinguishable peaks in the O K-edge spectrum for gibbsite (Figure 3b), one (I) at 535 eV and another one (II) at 540 eV, that can be assigned to σ^* transitions of Al–O and O–H bonding.[32] The combination of surface sensitive Al and O K-edge XAS therefore demonstrates that the bulk gibbsite structure and chemistry was represented at the surface of the samples that were determined to be pure gibbsite from XRD, which is of significance when considering surface-mediated mineral transformations.

Particle size and morphology were strongly affected by temperature. SEM indicated the low temperature products contained irregular nanoparticles (Figure 4a,b), but, at greater temperature, the crystals took the form of uniform hexagonal nanoplates (Figure 4c–e), which was also confirmed by XRD. Figure 4f shows the HAADF STEM image of the gibbsite synthesized at 80 °C. The transition from rough irregular nanoparticles to a well-defined crystal habit may be explained by the greater degree of supersaturation in low temperature runs, which promotes disordered crystal growth.[31] In particular, gibbsite crystal growth has been reported to occur through a screw dislocation growth mechanism at low supersaturation and by a two-dimensional nucleation growth mechanism at higher supersaturation.[18] Furthermore, the greater temperature enables kinetic bottlenecks to be more readily and thus yields morphologies closer to the equilibrium morphology. Among these more successful runs at greater temperatures, a statistical

DOI: 10.1021/acs.cgd.7b01400
Cryst. Growth Des. 2017, 17, 6801–6808

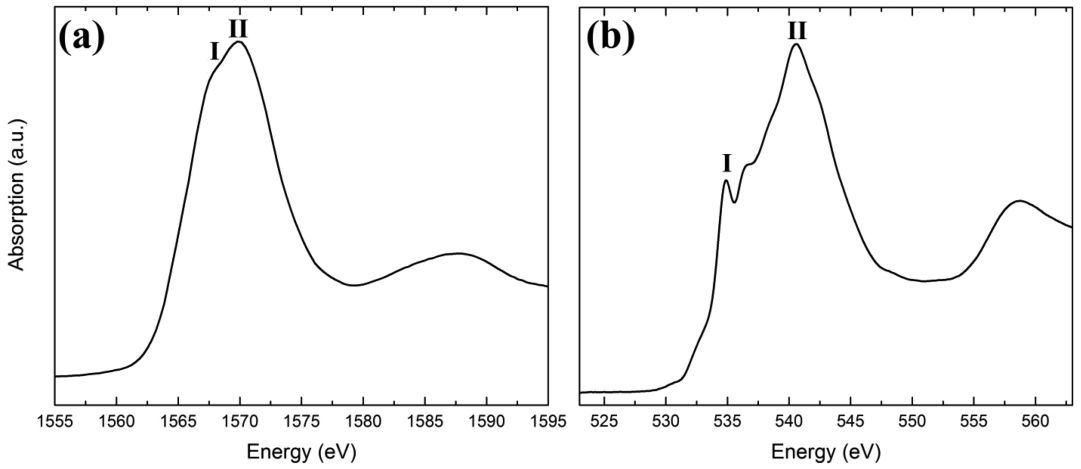

Figure 3. Al (a) and O (b) K-edge spectra of gibbsite synthesized at 80 °C for 72 h.

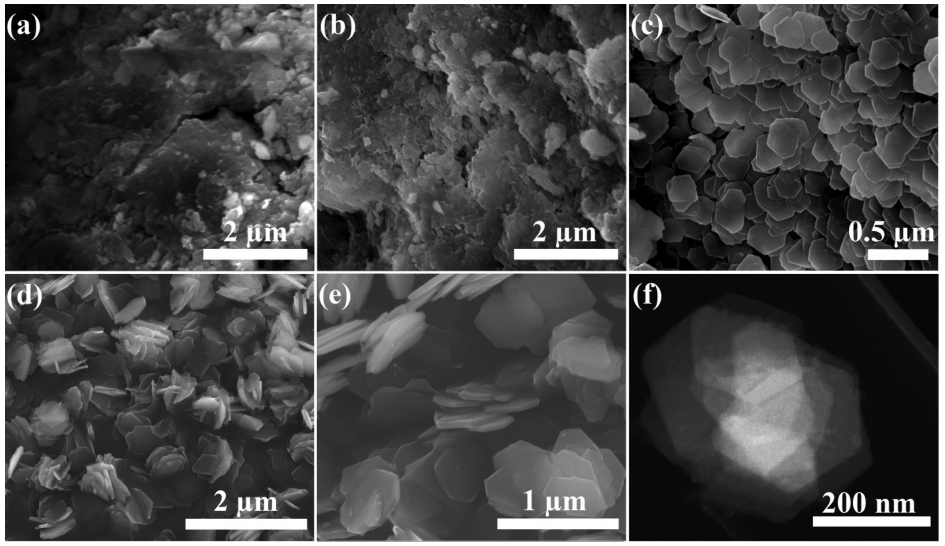

Figure 4. SEM images of gibbsite synthesized at (a) 60; (b) 70; (c) 80; (d) 90; and (e) 100 °C for 72 h. (f) HAADF STEM image of gibbsite synthesized at 80 °C for 72 h.

analysis of particle size from the SEM imaging data indicated the nanoplates systematically increased in diameter from 280 ± 35 to 369 ± 51 nm with increasing temperature from 80 to 100 °C, respectively (Table 1, entries 3−5). Furthermore, the fwhm of the (0 0 2) diffraction fits was used to estimate the gibbsite nanoplate thickness via using the Debye−Scherrer formula. As shown in Figure S2, the average thickness of as-synthesized gibbsite increased with increasing hydrothermal temperature. The average thickness of gibbsite was around 13 nm when the temperature was 60 °C, but the thickness changed to 29 nm when the temperature increased to 100 °C. AFM was also used to study the thickness of gibbsite nanoplates synthesized at greater temperatures (80−100 °C). As shown in Figure S3, nanoplate thickness also systematically increased with increasing the temperature. The average thickness was around 18 and 26 nm when the temperature was 80 and 100 °C, respectively, which agrees well with the XRD measurement.. Because the smallest possible high-purity nanoplates are desired for most applications of interest, we selected 80 °C as the optimal temperature for exploring the effects of other system variables.

Effect of Reaction Time. For the synthesis temperature of 80 °C, we next examined the effect of reaction time (Table 1, entries 3, 6−9). With respect to product yield, not surprisingly, only a minimal amount of crystalline product appeared after short reaction times (12 and 24 h). The yield increased substantially and systematically from 29% to 83% when the reaction time was increased to 48 h and then to 72 h. However, there was no obvious additional increase in yield when the reaction time was extended to 96 h. XRD indicated that samples collected at 48, 72, and 96 h were pure gibbsite. SEM showed that the morphologies of all these three samples were hexagonal nanoplates with sizes from 200 to 400 nm (Figures 4C and S4). The increase in yield between 12 and 72 h is consistent with continuous precipitation of soluble aluminate species. Because the 72 h reaction time produced the finest particle size and highest yield, this was taken as the reaction time of choice for investigating the effect of pH on product characteristics.

Effect of pH. For 80 °C and 72 h, we examined seven different pH values, 1, 3, 5, 7, 10, 12, and 13.5, as shown inTable 1 (entries 3, 10−15). XRD analyses indicated samples synthesized from pH 1 to 12 were pure gibbsite (Figures 1C and S5). However, the sample synthesized at pH 13.5 was a mixture of 70% gibbsite and 30% bayerite (ICDD PDF # 00-

DOI: 10.1021/acs.cgd.7b01400
Cryst. Growth Des. 2017, 17, 6801−6808

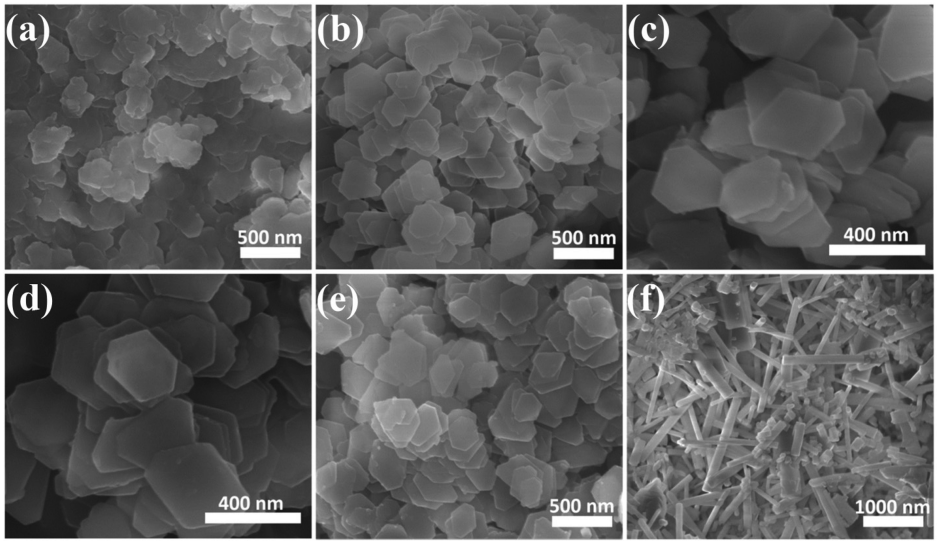

Figure 5. SEM images of as-prepared gibbsite at different pH values: (a) 1; (b) 3; (c) 5; (d) 10; (e) 12; and (f) 13.5.

20-0011) (Figure S5e). SEM analysis showed that the samples synthesized from pH 3 to 12 maintained a hexagonal nanoplate shape with diameters of 200−400 nm (Figures 3c and 5b−e). But the sample synthesized at pH 1 consisted of nanoplates with irregular edges (Figure 5a), and the gibbsite fraction of the product synthesized at pH 13.5 was made of bar-shaped crystals with lengths up to several micrometers (Figure 5f). Although highly acidic conditions can also be used to prepare gibbsite nanoplates, the reaction yield was much lower than in highly basic conditions (Table 1, entries 3, 10−15). Generally pH influences the morphology and yield of gibbsite through a variety of mechanisms including modulating aluminum ion cluster and aluminate speciation in solution,[35−37] sorption and stabilization of crystal facets,[38] and by influencing cluster−cluster and colloid−colloid interactions and aggregation through variation of the ionic strength of the solution.[19] At the extreme pH of 13.5, the chemical potential of OH^- may be high enough to adsorb on the normally unreactive (001) face and thereby inhibit further growth along the direction normal to that plane, yielding preferential growth along {110} and {100} faces and the observed bar shape morphology. At lower pH, the ability of OH^- to adsorb and "pin" the (001) face is diminished, therefore the normal tabular crystal growth habit manifests. Furthermore, no significant change in yield was found from pH 5 to 12, and pH 7 was thus selected for further work on the effect of precursor concentration.

Yield Optimization Based on Statistical Experimental Design. Gibbsite characteristics that resulted from the exploration of temperature, time, and pH synthesis conditions led to the identification of desirable conditions for morphologically well-defined nanoplates. For example, temperature was the most important factor to control the particle size. While low temperatures always yielded small particles, a temperature of 80 °C was required to obtain small and uniform gibbsite nanoplates at reasonable yields. However, to extend these insights into consideration of optimizing product yield, we also needed to examine the primary yield-limiting role of precursor concentration. Five different concentrations of gel, (0.1, 0.2, 0.5, 0.75, and 1.0 M) were investigated (Table 1, entries 3, 16−19). XRD confirmed that in all cases the product was pure gibbsite (Figures 1C and S6). SEM confirmed no obvious influence on particle size and shape, except for the samples synthesized with 0.75 and 1 M precursor concentrations, which yielded particles mildly irregular in shape either intrinsically or more likely as a result of being coated with trace residual unreacted gel (Figure S7) (a visible excess gel was recovered from these higher concentration experiments). We thus excluded these two highest concentrations from further consideration.

On the basis of application of a statistical analysis approach applied to the 80 °C temperature choice reaction time, pH, and precursor concentration were utilized in a statistical analysis to optimize the yield. The optimal conditions were determined using a three-factor and three-level BBD approach that made use of the experimental yields obtained at 0.2, 0.35, and 0.5 M for the precursor concentrations, 5, 8.5, and 12 for the pH, and 40, 56, and 72 h for the reaction time.[28,29,39] The response value of the reaction yield was found to range from 6 to 87% in Table 2.

The ANOVA of reaction yield for the nanoplates is given in Table S2. The model F value of 22.1 and low p-value of 0.002 imply that the model is significant. Moreover, the most significant factor is time, while the factor of concentration is insignificant. The good predictability of the models is indicated by correlation coefficient (R^2) of 0.976. This result means that 97.6% of the total variation on product yield data can be described by the selected model.

The mathematical equation for predicting the optimum point between the three variables in the coded levels and the response can be expressed as follows:

$$Y = 44.7192 - 0.87991X_1 - 5959X_2 + 29.1514X_3 - 4.7889{X_1}^2 - 12.1333{X_2}^2 + 0.5058X_1X_2 + 5.6471X_1X_3 - 4.2354X_2X_3$$

where Y, X_1, X_2, X_3 represent reaction yield, gel concentration, pH, and time, respectively.

Coefficients of one factor in the equation indicate the effect of the particular factor, whereas coefficients of two factors and second-order terms indicate the interaction between the three factors and a quadratic effect, respectively. The positive sign in front of the terms represents a synergistic effect, while a negative sign represents an antagonistic effect.

DOI: 10.1021/acs.cgd.7b01400
Cryst. Growth Des. 2017, 17, 6801−6808

Table 3. Optimal Factors and the Experimental Verification Value

			yield (%)	
gel concentration (M)	pH	time (h)	predict	experimental
0.5	9.2	72	87.77	88

On the basis of the results of BBD experiment, together with the quadratic equation fitting of these three variables of gel concentration, pH, and time, the predicted response value of the reaction yield was around 88%, and the optimal combination of each factor was determined by Minitab software. The prediction of the statistical analysis was confirmed experimentally, as shown in Table 4.

CONCLUSIONS

We have developed a new hydrothermal method to rapidly prepare euhedral hexagonal gibbsite nanoplates within a diameter range of 200−400 nm from an $Al(OH)_3$ gel precursor. The new synthesis involves very simple procedures. The separate effects of gel concentration, pH, and time on the reaction yield were investigated using a statistical design approach. The *p*-value, *F* statistics, and R^2 statistics of ANOVA show that the models can adequately describe the data and all three factors influence the response of reaction yield. The optimum synthesis conditions obtained by the BBD optimization tool for the predicted models were tested, and it was found that the experimental and predicted values were in excellent agreement. At 80 °C, the optimum synthesis conditions of gel concentration at 0.5 M, pH at 9.2, and time at 72 h maximized the reaction yield up to ∼88%. On the basis of these optimized experimental conditions, the synthesis procedure, which is both cost-effective and environmentally friendly, has the potential for scale-up for mass production of high quality gibbsite material for various research and development, and industrial applications.

ASSOCIATED CONTENT

Supporting Information

The Supporting Information is available free of charge on the ACS Publications website at DOI: 10.1021/acs.cgd.7b01400.

Crystal structure of gibbsite; crystalline size and composition analysis of gibbsite synthesized at different temperature; AFM images of gibbsite synthesized at 80 and 100 °C; SEM images of gibbsite synthesized at different reaction times and precursor concentrations; XRD patterns of gibbsite synthesized at different pH and precursor concentrations; experimental table for Box-Behnken Design; ANOVA for response of dependent variables (PDF)

AUTHOR INFORMATION

Corresponding Authors

*E-mail: kevin.rosso@pnnl.gov (K.M.R.).
*E-mail: xin.zhang@pnnl.gov (X.Z.).

ORCID

Sebastien Kerisit: 0000-0002-7470-9181
Kevin M. Rosso: 0000-0002-8474-7720

Notes

The authors declare no competing financial interest.

ACKNOWLEDGMENTS

This work was supported by IDREAM (Interfacial Dynamics in Radioactive Environments and Materials), an Energy Frontier Research Center funded by the U.S. Department of Energy (DOE), Office of Science, Basic Energy Sciences (BES). The authors acknowledge fruitful discussions with Mark Bowden on the XRD data analysis. A portion of this research was performed using EMSL, a national scientific user facility sponsored by the DOE Office of Biological and Environmental Research and located at Pacific Northwest National Laboratory (PNNL). PNNL is a multiprogram national laboratory operated for DOE by Battelle Memorial Institute under Contract No. DE-AC06-76RLO-1830. The work performed at the Advanced Light Source (ALS) was supported by the Director, Office of Science, BES of the DOE under Contract No. DE-AC02-05CH11231.

REFERENCES

(1) Yen, Y.-Y.; Wang, H.-T.; Guo, W.-J. Synergistic effect of aluminum hydroxide and nanoclay on flame retardancy and mechanical properties of EPDM composites. *J. Appl. Polym. Sci.* **2013**, *130*, 2042−2048.

(2) Huittinen, N.; Rabung, T.; Lutzenkirchen, J.; Mitchell, S. C.; Bickmore, B. R.; Lehto, J.; Geckeis, H. Sorption of Cm(III) and Gd(III) onto gibbsite, alpha-$Al(OH)_3$: A batch and TRLFS study. *J. Colloid Interface Sci.* **2009**, *332*, 158−164.

(3) Louaer, S.; Wang, Y.; Guo, L. Fast synthesis and size control of gibbsite nanoplatelets, their pseudomorphic dehydroxylation, and efficient dye adsorption. *ACS Appl. Mater. Interfaces* **2013**, *5*, 9648−9655.

(4) Weerasooriya, R.; Seneviratne, W.; Kathriarachchi, H. A.; Tobschall, H. J. Thermodynamic assessment of Hg(II)-gibbsite interactions. *J. Colloid Interface Sci.* **2006**, *301*, 452−460.

(5) Weerasooriya, R.; Tobschall, H. J.; Wijesekara, H. K. D. K.; Arachchige, E. K. I. A. U. K.; Pathirathne, K. A. S. On the mechanistic modeling of As(III) adsorption on gibbsite. *Chemosphere* **2003**, *51*, 1001−1013.

(6) Shi, Y.; HogenEsch, H.; Regnier, F. E.; Hem, S. L. Detoxification of endotoxin by aluminum hydroxide adjuvant. *Vaccine* **2001**, *19*, 1747−1752.

(7) Ulanova, M.; Tarkowski, A.; Hahn-Zoric, M.; Hanson, L. A. The Common vaccine adjuvant aluminum hydroxide up-regulates accessory properties of human monocytes via an interleukin-4-dependent mechanism. *Infect. Immun.* **2001**, *69*, 1151−1159.

(8) Santos, P. S.; Santos, H. S.; Toledo, S. P. Standard transition aluminas. Electron microscopy studies. *Mater. Res.* **2000**, *3*, 104−114.

(9) Reynolds, J. G.; Cooke, G. A.; Herting, D. L.; Warrant, R. W. Evidence for Dawsonite in Hanford high-level nuclear waste tanks. *J. Hazard. Mater.* **2012**, *209−210*, 186−192.

(10) Kumara, C. K.; Ng, W. J.; Bandara, A.; Weerasooriya, R. Nanogibbsite: synthesis and characterization. *J. Colloid Interface Sci.* **2010**, *352*, 252−258.

(11) Wijnhoven, J. E.; van't Zand, D. D.; van der Beek, D.; Lekkerkerker, H. N. Sedimentation and phase transitions of colloidal gibbsite platelets. *Langmuir* **2005**, *21*, 10422−10427.

(12) Li, H.; Addai-Mensah, J.; Thomas, J. C.; Gerson, A. R. The influence of Al(III) supersaturation and NaOH concentration on the rate of crystallization of $Al(OH)_3$ precursor particles from sodium aluminate solutions. *J. Colloid Interface Sci.* **2005**, *286*, 511−519.

(13) Cesteros, Y.; Salagre, P.; Medina, F.; Sueiras, J. E. A New Route to the Synthesis of Fine-Grain Gibbsite. *Chem. Mater.* **2001**, *13*, 2595−2600.

(14) Freij, S. J.; Parkinson, G. M. Surface morphology and crystal growth mechanism of gibbsite in industrial Bayer liquors. *Hydrometallurgy* **2005**, *78*, 246−255.

DOI: 10.1021/acs.cgd.7b01400
Cryst. Growth Des. 2017, 17, 6801−6808

(15) Freij, S. J.; Parkinson, G. M.; Reyhani, M. M. Atomic force microscopy study of the growth mechanism of gibbsite crystals. *Phys. Chem. Chem. Phys.* **2004**, *6*, 1049.
(16) Freij, S. J.; Parkinson, G. M.; Reyhani, M. M. Direct observation of the growth of gibbsite crystals by atomic force microscopy. *J. Cryst. Growth* **2004**, *260*, 232−242.
(17) Fu, W.; Vaughan, J.; Gillespie, A. Aspects of the Mechanism of Nucleation and Intergrowth of Gibbsite Crystals on Sodium Oxalate Surfaces in Concentrated Alkaline Solutions. *Cryst. Growth Des.* **2015**, *15*, 374−383.
(18) Li, T. S.; Livk, I.; Ilievski, D. Supersaturation and temperature dependency of gibbsite growth in laminar and turbulent flows. *J. Cryst. Growth* **2003**, *258*, 409−419.
(19) Sweegers, C.; De Coninck, H. C.; Meekes, H.; Van Enckevort, W. J. P.; Hiralal, I. D. K.; Rijkeboer, A. Morphology, evolution and other characteristics of gibbsite crystals grown from pure and impure aqueous sodium aluminate solutions. *J. Cryst. Growth* **2001**, *233*, 567−582.
(20) Wierenga, A. M.; Lenstra, T. A.; Philipse, A. P. Aqueous dispersions of colloidal gibbsite platelets- synthesis, characterisation and intrinsic viscosity measurements. *Colloids Surf., A* **1998**, *134*, 359−371.
(21) Wijnhoven, J. E. Seeded growth of monodisperse gibbsite platelets to adjustable sizes. *J. Colloid Interface Sci.* **2005**, *292* (2), 403−409.
(22) Peskleway, C. D.; Henderson, G. S.; Wicks, F. J. Dissolution of gibbsite: Direct observations using fluid cell atomic force microscopy. *Am. Mineral.* **2003**, *88*, 18−26.
(23) Liu, Y.; Ma, D.; Blackley, R. A.; Zhou, W.; Han, X.; Bao, X. Synthesis and characterization of gibbsite nanostructures. *J. Phys. Chem. C* **2008**, *112*, 4124−4128.
(24) van der Beek, D.; Lekkerkerker, H. N. Liquid crystal phases of charged colloidal platelets. *Langmuir* **2004**, *20*, 8582−8586.
(25) Shen, S.; Chow, P. S.; Chen, F.; Feng, S.; Tan, R. B. H. Synthesis of submicron gibbsite platelets by organic-free hydrothermal crystallization process. *J. Cryst. Growth* **2006**, *292*, 136−142.
(26) Hiemstra, T.; Yong, H.; Van Riemsdijk, W. H. Interfacial charging phenomena of aluminum (hydr) oxides, Interfacial Charging Phenomena of Aluminum (Hydr)oxides. *Langmuir* **1999**, *15*, 5942−5955.
(27) Rosenqvist, J.; Persson, P.; Sjöberg, S. Protonation and charging of nanosized gibbsite (α-$Al(OH)_3$) particles in aqueous suspension. *Langmuir* **2002**, *18*, 4598−4604.
(28) Bingöl, D.; Veli, S.; Zor, S.; Özdemir, U. Analysis of adsorption of reactive azo dye onto $CuCl_2$ doped polyaniline using Box−Behnken design approach. *Synth. Met.* **2012**, *162*, 1566−1571.
(29) Ba-Abbad, M. M.; Chai, P. V.; Takriff, M. S.; Benamor, A.; Mohammad, A. W. Optimization of nickel oxide nanoparticle synthesis through the sol−gel method using Box−Behnken design. *Mater. Des.* **2015**, *86*, 948−956.
(30) Ildefonse, P.; Cabaret, D.; Sainctavit, P.; Calas, G.; Flank, A. M.; Lagarde, P. Aluminum X-ray absorption near edge structure in model compounds and earth's surface minerals. *Phys. Chem. Miner.* **1998**, *25*, 112−121.
(31) Sonthalia, R.; Behara, P.; Kumaresan, T.; Thakre, S. Review on alumina trihydrate precipitation mechanisms and effect of Bayer impurities on hydrate particle growth rate. *Int. J. Miner. Process.* **2013**, *125*, 137−148.
(32) Hu, Y. F.; Xu, R. K.; Dynes, J. J.; Blyth, R. I. R.; Yu, G.; Kozak, L. M.; Huang, P. M. Coordination nature of aluminum (oxy)hydroxides formed under the influence of tannic acid studied by X-ray absorption spectroscopy. *Geochim. Cosmochim. Acta* **2008**, *72*, 1959−1969.
(33) Saalfeld, H.; Wedde, M. Refinement of the crystal structure of gibbsite, $Al(OH)_3$. *Z. Kristallogr.* **1974**, *139*, 129−135.
(34) Stohr, J. *NEXAFS Spectroscopy*; Springer: New York, USA, 1992.
(35) Casey, W. H. Large aqueous aluminum hydroxide molecules. *Chem. Rev.* **2006**, *106*, 1−16.
(36) Swaddle, T. W.; Rosenqvist, J.; Yu, P.; Bylaska, E.; Phillips, B. L.; Casey, W. H. Kinetic evidence for five-coordination in AlOH (aq) 2+ ion. *Science* **2005**, *308*, 1450−1453.
(37) Casey, W. H.; Phillips, B. L.; Furrer, G. Aqueous aluminum polynuclear complexes and nanoclusters: a review. *Rev. Mineral. Geochem.* **2001**, *44*, 167−190.
(38) Preocanin, T.; Abdelmonem, A.; Montavon, G.; Luetzenkirchen, J. Charging Behavior of Clays and Clay Minerals in Aqueous Electrolyte Solutions — Experimental Methods for Measuring the Charge and Interpreting the Results. *Clays, Clay Minerals and Ceramic Materials Based on Clay Minerals* **2016**, 51−88.
(39) Ferreira, S. L.; Bruns, R. E.; Ferreira, H. S.; Matos, G. D.; David, J. M.; Brandao, G. C.; da Silva, E. G.; Portugal, L. A.; dos Reis, P. S.; Souza, A. S.; dos Santos, W. N. Box-Behnken design: an alternative for the optimization of analytical methods. *Anal. Chim. Acta* **2007**, *597*, 179−186.

DOI: 10.1021/acs.cgd.7b01400
Cryst. Growth Des. 2017, 17, 6801−6808